Centrality dependence of the direct photon yield and elliptic flow in heavy-ion collisions at $\sqrt{s_{NN}} = 200$ GeV

O. Linnyk,* and W. Cassing
Institute for Theoretical Physics, Justus Liebig University of Giessen, 35392 Giessen, Germany

E. L. Bratkovskaya
Institute for Theoretical Physics, Johann Wolfgang Goethe University, 60438 Frankfurt am Main, Germany and Frankfurt Institute for Advanced Studies, 60438 Frankfurt am Main, Germany

(Received 18 January 2014; revised manuscript received 20 February 2014; published 19 March 2014)

We calculate the centrality dependence of direct photons produced in Au+Au collisions at the invariant collision energy $\sqrt{s_{NN}} = 200$ GeV and their transverse momentum spectra within the parton-hadron-string dynamics transport approach. As sources for "direct" photons, we incorporate the interactions of quarks and gluons as well as hadronic interactions ($\pi + \pi \to \rho + \gamma$, $\rho + \pi \to \pi + \gamma$, meson-meson bremsstrahlung $m + m \to m + m + \gamma$, and meson-baryon bremsstrahlung $m + B \to m + B + \gamma$), the decays of ϕ and a_1 mesons, and the photons produced in the initial hard collisions. We find that the transverse momentum p_T spectra of the "thermal" photons (i.e., the direct photons after the pQCD contribution is subtracted) deviate from exponential distributions and, consequently, observe a strong dependence of the inverse slope parameter $T_{\rm eff}$ on the fitting range in p_T. On the other hand, all the obtained "effective temperatures" are well above the critical temperature for the deconfinement phase transition even for peripheral collisions, reflecting primarily a "blue shift" due to radial collective motion of hadrons. Our calculations suggest that the channel decomposition of the observed spectrum changes with centrality with an increasing (dominant) contribution of hadronic sources for more peripheral reactions. Furthermore, the thermal photon yield is found to scale roughly with the number of participant nucleons as $N_{\rm part}^{\alpha}$ with $\alpha \approx 1.5$, whereas the partonic contribution scales with an exponent $\alpha_p \approx 1.75$. Additionally, we provide predictions for the centrality dependence of the direct photon elliptic flow $v_2(p_T)$. The photons from the hot deconfined matter in the early stages of the collision carry a much smaller elliptic flow than the final hadrons. Consequently, the direct photon v_2 in the most central bin is of the order of a few percent. On the other hand, the elliptic flow of direct photons is considerably larger in more peripheral collisions, approaching that of hadrons.

DOI: 10.1103/PhysRevC.89.034908 PACS number(s): 25.75.−q, 13.85.Qk, 24.85.+p

I. INTRODUCTION

The "direct photons" from relativistic heavy-ion collisions are a valuable probe of the collision dynamics at early times and provide information on the characteristics of the initially created matter once the final state hadronic decay photons are subtracted from the experimental spectra [1–7]. In the last years, the PHENIX Collaboration [8–11] has measured the spectra of the photons produced in minimal bias Au+Au collisions at the invariant collision energy $\sqrt{s_{NN}} = 200$ GeV and found a strong elliptic flow $v_2(p_T)$ of direct photons, which is comparable to that of the produced pions. Since direct photons were expected to be essentially produced in the initial hot medium before the collective flow has developed, this observation was in contrast to the theoretical expectations and predictions [12–16]. Also more recent studies employing event-by-event hydrodynamical calculations [17–19] severely have underestimated the elliptic flow of direct photons, and alternative sources of direct photons from the conformal anomaly have been suggested [20]. Furthermore, in order to distinguish direct photons from the strong magnetic field of spectator protons (due to the conformal anomaly) it has been suggested to explore the centrality dependence of the direct photon v_2 in correlation with the elliptic flow from pions [21].

On the other hand, in Ref. [22] we have proposed that apart from the partonic production channels the direct photon yield and primarily the strong v_2 might be due to hadronic sources (such as meson-meson Bremsstrahlung or hadronic interactions as $\pi + \pi \to \rho + \gamma$, $\rho + \pi \to \pi + \gamma$, etc.). Indeed, the interacting hadrons carry a large v_2 and contribute by more than 50% to the measured direct photons according to the parton-hadron-string dynamics (PHSD) calculations in Ref. [22] (cf. also the hydrodynamics calculations in Ref. [23]). For a quantitative understanding of the direct photon production it is important to verify the decomposition of the total photon yield according to the production sources: the late hadron decays (the cocktail), hadronic interactions beyond the cocktail (during the collision phase), and the partonic interactions in the quark-gluon plasma (QGP). Since previous transport studies have indicated that the duration of the partonic phase substantially decreases with increasing impact parameter (cf. Fig. 4 in Ref. [24]) we will study here explicitly the centrality dependence of the direct photon yield together with the essential production channels and their impact on the photon v_2.

As in Ref. [22] we will employ the PHSD transport approach to investigate the photon production in Au+Au collisions at $\sqrt{s_{NN}} = 200$ GeV at various centralities thus extending our previous investigations for the case of minimum bias collisions. We recall that the PHSD approach has provided a consistent description of the bulk properties of heavy-ion collisions—rapidity spectra, transverse mass distributions, and

*Olena.Linnyk@theo.physik.uni-giessen.de

azimuthal asymmetries of various particle species—from low Super Proton Synchrotron (SPS) to top Relativistic Heavy Ion Collider (RHIC) energies [25] and was successfully used also for the analysis of dilepton production from hadronic and partonic sources at SPS, RHIC, and Large Hadron Collider (LHC) energies [26]. It is therefore of interest to calculate also the photon production in relativistic heavy-ion collisions from hadronic and partonic interactions within the PHSD transport approach, since its microscopic and nonequilibrium evolution of the nucleus-nucleus collision is independently controlled by a multitude of other hadronic and electromagnetic observables in a wide energy range [24–27].

II. PHOTONS WITHIN PHSD

For the details on the PHSD approach we refer the reader to Refs. [25,28] and the implementation of the photon production to Refs. [22,29] (and references therein). Let us recall that the dynamical calculations within the PHSD have reproduced the measured differential spectra of dileptons produced in heavy-ion collisions at SPS and RHIC energies (see Ref. [26]). Furthermore, the dilepton production rate from the QGP constituents—as incorporated in the PHSD—agrees with the dilepton rate from the thermalized QCD medium as calculated by lattice QCD (lQCD). We note, additionally, that the electric conductivity of the QGP from the PHSD, which controls the photon emission rate in equilibrium, is rather well in line with available lQCD results [30].

As sources of photon production—on top of the general dynamical evolution—we consider hadronic [29,31–33] as well as partonic [2,4,34–36] interactions. In the present study we extend the calculations in Ref. [22] by adding an additional source of photons, i.e., the bremsstrahlung in elastic meson-baryon collisions ($m + B \to m + B + \gamma$). In our previous study (Ref. [22]), we have considered the meson-meson bremsstrahlung, because it had been proposed to be important already in Refs. [29,33]. At the time we had not realized the potential importance of the photon production in meson-baryon collisions. However, we will see below that this process contributes considerably.

The bremsstrahlung production of photons inmeson-meson and meson-baryon collisions is calculated using the soft photon approximation as in Refs. [22,29,33,37]. The soft-photon approximation (SPA) relies on the assumption that the radiation from internal lines is negligible and the strong interaction vertex is on-shell. In this case the strong interaction part and the electromagnetic part can be separated, so the soft-photon cross section for the reaction $h_1 + h_2 \to h_1 + h_2 + \gamma$ (where h_i denote colliding hadrons) can be written as

$$q_0 \frac{d^3\sigma^\gamma}{d^3q} = \frac{\alpha}{4\pi} \frac{\bar{\sigma}(s)}{q_0^2}, \qquad \bar{\sigma}(s) = \frac{s - (M_1 + M_2)^2}{2M_1^2} \sigma(s), \tag{1}$$

where M_1 is the mass of the charged accelerated particle; M_2 is the mass of the second particle; q_0 and q are the photon energy and momentum, respectively. In (1) $\sigma(s)$ is the on-shell cross section for the reaction $h_1 + h_2 \to h_1 + h_2$, i.e., the elastic scattering of the two hadrons.

Let us point out that the resulting yield of the bremsstrahlung photons depends on the model assumptions such as the cross sections for the meson-meson and meson-baryon elastic scatterings, incoherence of the individual scatterings, and the soft photon approximation. The theoretical uncertainty of up to a factor of 2 due to the unmeasured elastic scattering cross sections has to be kept in mind. The adequacy of the SPA assumption has been checked in Ref. [37]. We recall here that the soft photon approximation is no longer valid for high energies of the produced photons or at high $\sqrt{s}$ of the meson-meson or meson-baryon collisions [38]. Thus we have restricted our kinematics by considering only meson-meson and baryon-meson collisions with available energies $\sqrt{s}$ below 3 GeV. Our conclusions on the centrality dependence of the direct photons are not sensitive to the actual value of this cutoff within reasonable variations.

The assumption of incoherent photon production in individual hadron-hadron collisions is not applicable at very low transverse momenta of the photons. The Landau-Pomeranchuk-Migdal (LPM) effect is the suppression of bremsstrahlung photon emission due to the multiple scattering of the production source (in this case meson or baryon) during the time needed for the formation of the radiated photon. In this case the bremsstrahlung amplitudes interfer destructively. For the hadronic bremsstrahlung, the LPM effect in the thermal medium has been calculated in Ref. [39]. The suppression depends on the length of the formation zone of the photon, $z(\gamma)$, which is defined by the uncertainty principle and depends on the energy of the photon. The suppression becomes significant for photon energies below a certain value, for which $z(\gamma)$ becomes larger than the mean free path of the hadron, λ [40,41]. For the photon at midrapidity, $z(\gamma) = 2\omega/p_T^2 = 2/p_T$. On the other hand, the mean free path of the hadrons $\lambda = 1/(\sigma n)$ is governed by the hadronic scattering cross section (typically of the order of $\sigma = 20$ mb) and the hadron density n, which after the hadronization does not exceed $n_{\max} = 0.5$ fm^{-3}. Accordingly, the suppression due to the LMP effect is expected to be important for these processes at $p_T < 0.4$ GeV, where, however, no data are available yet. At present, we do not include the LMP effect on the bremsstrahlung photon production in our calculations due to the lack of data at sufficiently low p_T.

Since a new production mechanism has been added to the hadronic production channels (the meson-baryon bremsstrahlung), we first check whether this addition does not lead to an overestimation of the data from the PHENIX Collaboration [9,10] in minimal bias Au+Au collisions in Fig. 1. Since the decays of mesons as "late" hadronic sources are less sensitive to the creation of the hot and dense medium and to its properties, they are subtracted experimentally from the total photon yield to access the "direct" photon spectrum. In our calculations of the direct photon spectrum in Fig. 1 the following sources are taken into account: the decays of ω, η', ϕ, and a_1 mesons; the reactions $\pi + \rho \to \pi + \gamma, \pi + \pi \to \rho + \gamma$; the photon bremsstrahlung in meson-meson and meson-baryon collisions $m + m \to m + m + \gamma$, $m + B \to m + B + \gamma$; photon production in the QGP in the processes $q + \bar{q} \to g + \gamma$, and $q(\bar{q}) + g \to q(\bar{q}) + \gamma$ as well as the photon production in the initial hard collisions ("pQCD"), which is given by the

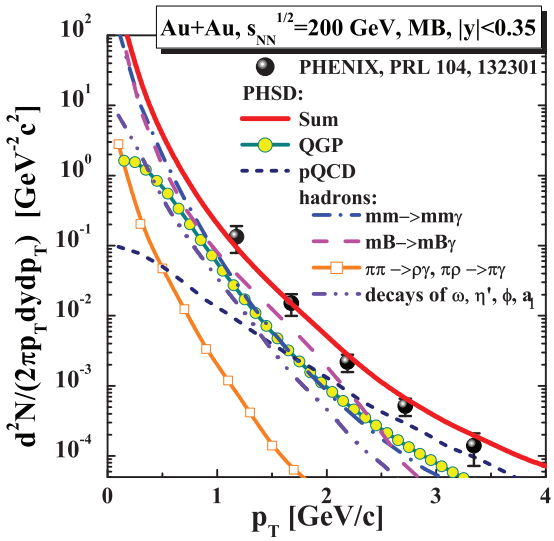

FIG. 1. (Color online) Direct photons (sum of all photon production channels except the π- and η-meson decays) from the PHSD approach (red solid line) in comparison to the data of the PHENIX Collaboration [9,10] for minimal bias collisions of Au+Au at $\sqrt{s_{NN}} = 200$ GeV (black symbols). The various channels are described in the legend.

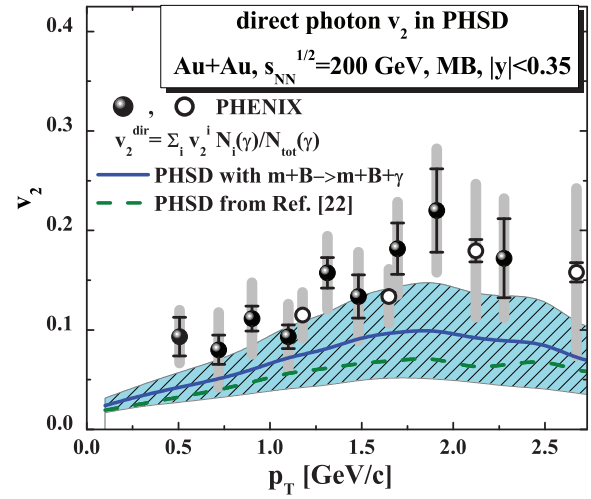

FIG. 2. (Color online) Direct photon elliptic flow (contributions from hadronic decays are subtracted) from the PHSD approach in comparison to the data of the PHENIX Collaboration [9,10] for minimal bias collisions of Au+Au at $\sqrt{s_{NN}} = 200$ GeV (black symbols). The green dashed line shows the PHSD results from Ref. [22] taking into account the following channels: $\pi + \rho \to \pi + \gamma, \pi + \pi \to \rho + \gamma$; the photon bremsstrahlung in meson-meson collisions $m + m \to m + m + \gamma$; photon production in the QGP in the processes $q + \bar{q} \to g + \gamma$, and $q(\bar{q}) + g \to q(\bar{q}) + \gamma$ as well as the photon production in the initial hard collision (pQCD). The blue solid line gives the results of the present calculations taking into account additionally the baryon-meson bremsstrahlung $m + B \to m + B + \gamma$.

hard photon yield in $p + p$ collisions scaled with the number of binary collisions, $N_{\rm coll}$. We find that our PHSD calculations are in a reasonable agreement with the PHENIX data [9,10] and show a clear dominance of the hadronic production channels over the partonic channels for transverse momenta below about 0.7 GeV/c. In particular, the bremsstrahlung contributions are responsible for the "banana shape" spectrum and the strong increase for low p_T. On the other hand, this increase should be softened to some degree by the LPM effect. Accordingly, especially experimental data well below 1 GeV/c in p_T will be helpful in disentangling the various sources.

In Fig. 2, we show explicitly the elliptic flow v_2 of direct photons in minimum bias collisions in comparison to the data and the previous centrality integrated results also for (the green dashed line) from the Ref. [22]. Note that the photons from the decays of ω and η' mesons have been subtracted from the v_2 data by experimental methods. We calculated the direct photon v_2 as a sum of $v_2(i)$ of each individual contributed channel, weighted with the channel's contribution to the p_T spectrum. The considered channels are: $\pi + \rho \to \pi + \gamma$, $\pi + \pi \to \rho + \gamma$; the photon bremsstrahlung in meson-meson collisions $m + m \to m + m + \gamma$; photon production in the QGP in the processes $q + \bar{q} \to g + \gamma$, and $q(\bar{q}) + g \to q(\bar{q}) + \gamma$ as well as the photon production in the initial hard collisions (i.e. the "pQCD" photons). The new calculations include additionally the meson bremsstrahlung processes $m + B \to m + B + \gamma$ and are shown by the blue solid line. The agreement with experiment has slightly improved compared to Ref. [22].

III. RESULTS FOR DIFFERENT CENTRALITIES

The calculated results for the direct photon spectrum in Au+Au collisions at $\sqrt{s_{NN}} = 200$ GeV are presented in Fig. 3 for various centralities as functions of the transverse momentum p_T at midrapidity $|y| < 0.35$. The direct photons are obtained experimentally from the total photon spectrum by subtracting meson decay photons based on measured meson yields. Therefore, in this case we disregard all hadron decays except the ϕ,a_1 photonic decays, which are subleading. The following contributions are addressed as direct photons: the decays of ϕ and a_1 mesons; the reactions $\pi + \rho \to \pi + \gamma$, $\pi + \pi \to \rho + \gamma$; the photon bremsstrahlung in meson-meson and meson-baryon collisions $m + m \to m + m + \gamma$, $m + B \to m + B + \gamma$; photon production in the QGP in the processes $q + \bar{q} \to g + \gamma$, and $q(\bar{q}) + g \to q(\bar{q}) + \gamma$ as well as the pQCD photons produced in the initial hard collisions. The direct pQCD contributions dominate above $p_T \approx 2$ GeV/c.

The spectra of "thermal" photons are obtained from the direct photon spectra (channels listed above) by additionally subtracting the photons produced in the initial hard pQCD processes. The pQCD photons are not expected to have a thermal spectrum and practically give no contribution to the direct photon elliptic flow. The thermal photons in 0–20% central, 20–40% central, 40–60% central, and 60–92% central Au+Au collisions at $\sqrt{s_{NN}} = 200$ GeV within the PHSD approach are displayed in Fig. 4. We only specify the dominant channels in Fig. 4, i.e., the contributions from $m + m$ and $m + B$ bremsstrahlung as well as the QGP contribution which is seen to become low in more peripheral collisions.

Though the spectrum presented in Fig. 4 is obviously not exponential in the full momentum range especially due to

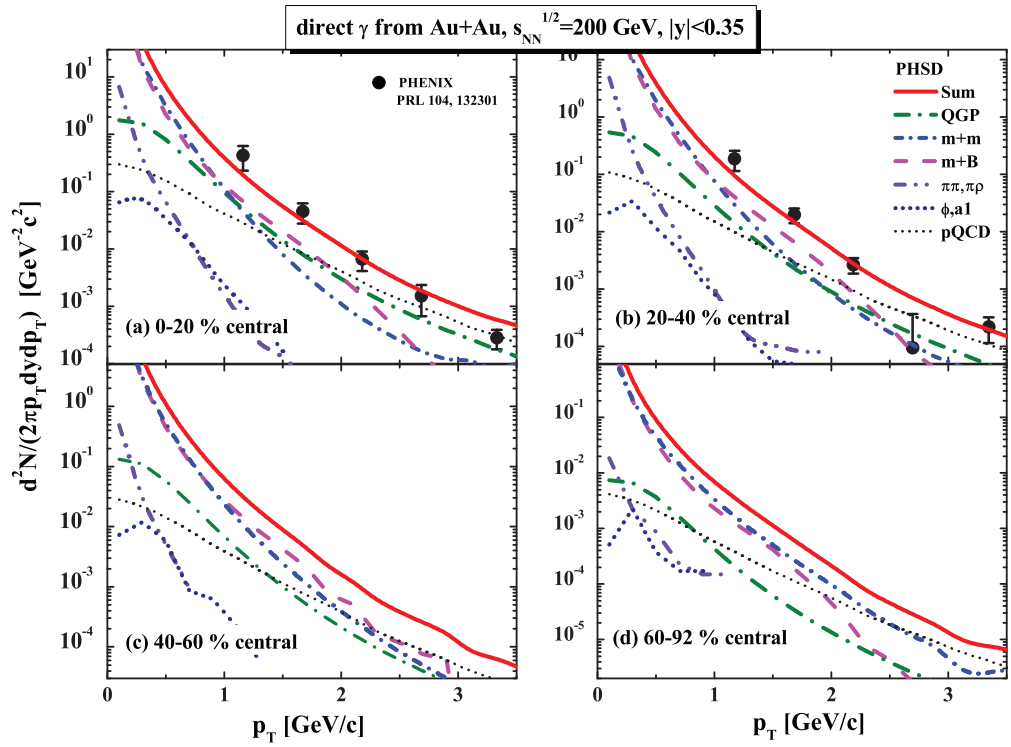

FIG. 3. (Color online) The channel decomposition of the direct photon transverse momentum p_T spectra for Au+Au collisions at $\sqrt{s_{NN}} = 200$ GeV (full solid upper line) at midrapidity $|y| < 0.35$ within the PHSD approach. The four panels present the results at various collision centralities: (a) 0–20% central, (b) 20–40% central, (c) 40–60% central, and (d) 60–92%. The channel description is given in the legend. The data are from [10].

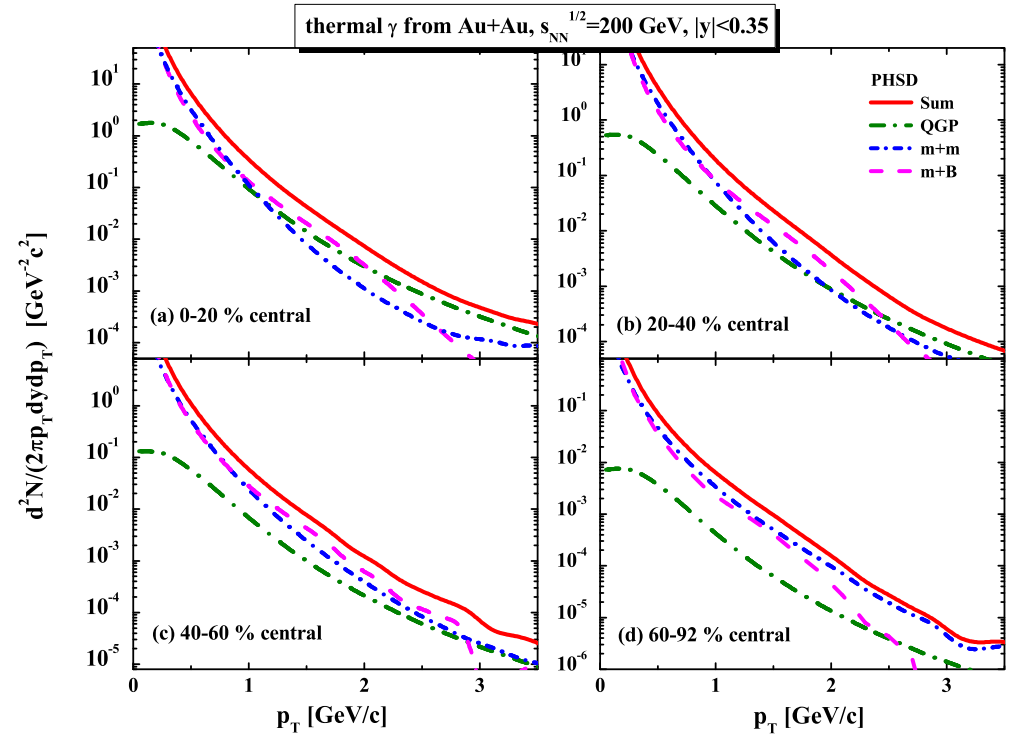

FIG. 4. (Color online) The spectra of thermal photons in (a) 0–20% central, (b) 20–40% central, (c) 40–60% central, and (d) 60–92% central Au+Au collisions at $\sqrt{s_{NN}} = 200$ GeV within the PHSD approach. In contrast to the plots in Fig. 3, we subtracted the contribution from the initial hard partonic collisions (the pQCD channel).

TABLE I. The slope parameter $T_{\rm eff}$ of the spectrum of thermal photons (Fig. 4) produced in Au+Au collisions at $\sqrt{s_{NN}} = 200$ GeV at various centralities. The value $T_{\rm eff}$ was obtained by approximating the spectrum by an exponential function in the transverse momentum range $0.6 < p_T < 2$ GeV.

Centrality	$N_{\rm part}$	$T_{\rm eff}$ (MeV)
0–20%	280	265 ± 20
20–40%	137	260 ± 20
40–60%	60	250 ± 20
60–92%	15	260 ± 20

the bremsstrahlungs channels, one may fit the spectra by exponentials in a finite transverse momentum region and define in this way an effective slope parameter or "effective temperature" as in the experimental analysis [9,10]. The slope of the transverse momentum spectrum of produced "thermal photons" is expected to give a glance at the initial temperatures reached in the collisions [2,4,12–15,18,31,32,42–48], and was even used to deduce an "average temperature" of the QGP [9,10]. We will present here the effective temperatures $T_{\rm eff}$ as extracted from the calculated transverse momentum spectra of thermal photons from Fig. 4, addressing them as "apparent inverse slope parameters" $T_{\rm eff}$ or energy scales for the photonic radiation. The extracted effective temperatures are shown in Table I at the different centralities for the transverse momentum interval 0.6–2 GeV. The "temperature" defined in this way depends on the fit range in transverse momentum and should only serve as a characteristic energy scale as mentioned above. Surprisingly, we find (within error bars) the same slope parameter $T_{\rm eff}$ which is significantly larger than the critical temperature $T_c \approx 160$ MeV for deconfinement. Since here the dominant contributions should be related to binary bremsstrahlung channels the high slope parameters predominantly reflect the "blue-shift" of the photon spectra due to the collective flow of hadrons (cf. Ref. [18]) which (for PHSD) was shown in Ref. [24] to be well in line with experimental observation.

Integrating the thermal photon spectra from Fig. 4 over the transverse momentum p_T in the interval $0.4 \leqslant p_T \leqslant 5\,{\rm GeV}/c$, we obtain the number of thermal photons (full squares) as a function of centrality, which is plotted in Fig. 5 as a function of the number of participants $N_{\rm part}$ calculated in the Monte-Carlo Glauber model described in Ref. [49]. Since only binary collision channels contribute to the production of thermal photons in our approach, their yield rises faster than $N_{\rm part}$ as expected from qualitative considerations in Refs. [50,51]. A power-law fit to our results gives approximately a scaling $\sim N_{\rm part}^{\alpha}$ with $\alpha \approx 1.5$. In addition we display in Fig. 5 the scalings with $N_{\rm part}$ for the partonic (full dots) and hadronic bremsstrahlung channels (full triangles) separately, which give exponents of $\approx$1.75 and $\approx$1.5, respectively.

As one can see in Figs. 3 and 4 qualitatively the contribution of the photons from the QGP is larger in central collisions while the hadronic sources contribute more dominantly in peripheral collisions. We quantify the relative contributions by plotting in Fig. 6 the ratio of the number of photons produced

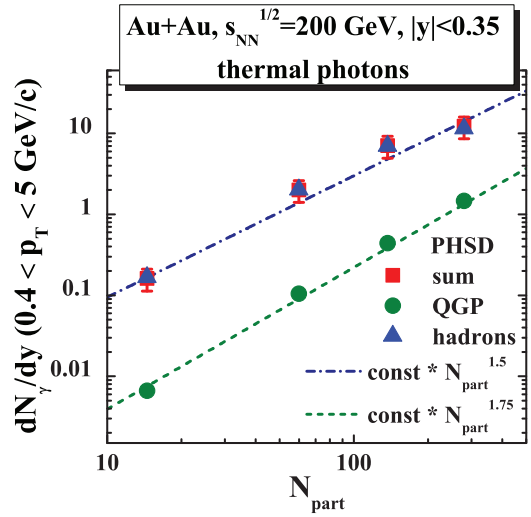

FIG. 5. (Color online) Integrated spectra of thermal photons (full squares) produced in Au+Au collisions at $\sqrt{s_{NN}} = 200$ GeV versus the number of participants $N_{\rm part}$. The scalings with $N_{\rm part}$ from the QGP contribution (full dots) and the bremsstrahlungs channels (full triangles) are shown separately.

in the QGP to the number of all direct photons (from the QGP, $m + m/B \to m + m/B + \gamma$, $\pi + \pi/\rho \to \rho/\pi + \gamma$, and the pQCD photons). The contribution of the QGP photons is seen to increase with transverse momentum and reaches slightly more than 30% for the most central event bin. On the other hand, the ratio of QGP photons to the total direct photons falls rapidly with decreasing centrality and is below 10% in the most peripheral centrality bin. Accordingly, minimal bias collisions are dominated by the hadronic channels that come along with a large hadronic elliptic flow v_2.

In Fig. 7 we provide predictions for the centrality dependence of the direct photon elliptic flow $v_2(p_T)$ within the PHSD approach. The direct photon v_2 is seen to be larger in the peripheral collisions compared to the most central ones.

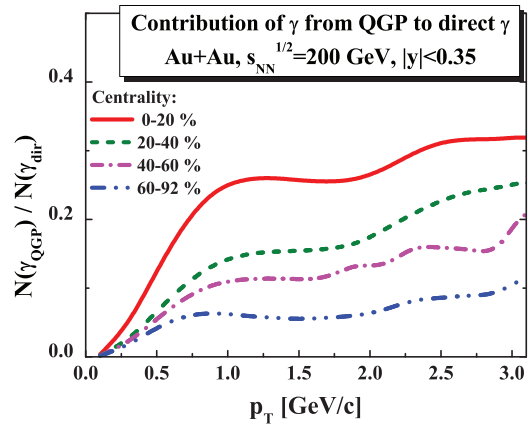

FIG. 6. (Color online) The ratios of the number of photons produced in the QGP to the number of all direct photons produced through binary processes in different-centrality Au+Au collisions at $\sqrt{s_{NN}} = 200$ GeV versus the photon transverse momentum p_T.

The predicted centrality dependence of the direct photon flow results from the interplay of two independent factors. First, the channel decomposition of the direct photon yield as presented by the ratios in Fig. 6 changes: the admixture of photons from the hadronic phase increases for more peripheral collisions. As has been described in detail in Ref. [22], the PHSD approach predicts a very small v_2 of photons produced in the initial hot deconfined phase by partonic channels of the order of 2%. On the other hand, the photons from the hadronic sources show strong elliptic flow (up to 10%), on the level of the v_2 of final hadrons [22]. Accordingly, since the channel decomposition of the direct photons changes with centrality, the elliptic flow of the direct photons increases with decreasing centrality and becomes roughly comparable with the elliptic flow of pions in peripheral collisions.

However, there is another (second) factor contributing to the centrality dependence of the photon elliptic flow. Let us recall the centrality dependence of the elliptic flow for charged particles, e.g., Fig. 7 of Ref. [24]. The v_2 rises almost linearly with increasing impact parameter b at small b, and decreases again in the most peripheral collisions. The latter decrease is a sign that the most peripheral collisions can be understood as a superposition of elementary collisions, with little collectivity. The elliptic flow of hadrons in PHSD in central and semicentral collisions grows with the impact parameter because of the growing ellipticity, which is transformed into the momentum anisotropy through the strong interaction within the quark-gluon plasma liquid in the initial stage of the collision. In contrast, the peripheral collisions in PHSD are dominated by hadron scatterings in the "corona," which do not produce large elliptic flow. Consequently, PHSD also predicts negligible elliptic flow in $p + A$ collisions. The special case of collisions with ultrahigh multiplicities is not considered in the present investigation. The elliptic flow of direct photons (presented in Fig. 7) in the most peripheral bin is low, because the particles have little flow at high impact parameter b.

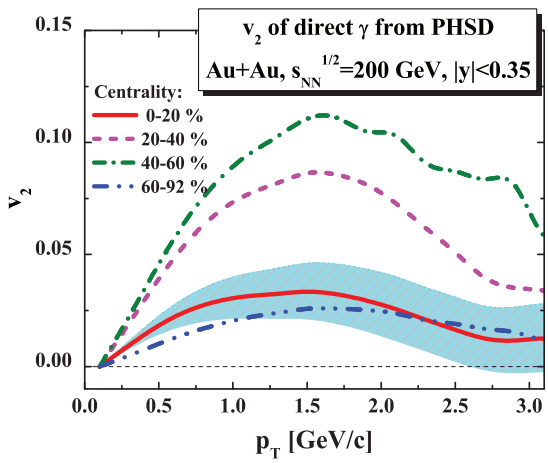

FIG. 7. (Color online) The elliptic flow $v_2(p_T)$ of direct photons produced through binary processes in Au+Au collisions at $\sqrt{s_{NN}} = 200$ GeV for different centralities versus the photon transverse momentum p_T. The hatched area (for the most central bin) stands for the statistical uncertainty in the photon v_2 from PHSD which in width is also characteristic for the other centralities.

This effect is present in the PHSD model as well as in the experimental observation.

IV. SUMMARY

The spectra of direct and thermal photons—as produced in Au+Au collisions at $\sqrt{s_{NN}} = 200$ GeV—have been calculated differentially in collision centrality within the PHSD transport approach, which has been previously tested in comparison to the measured spectra and flow of photons in minimal bias collisions at the same energy [22]. We have found that the channel decomposition of the photon spectra changes with centrality, with a larger contribution of the hadronic sources in more peripheral collisions.

As a consequence, the direct photon v_2 is larger in peripheral collisions as compared to the most central reactions. We recall that v_2 of photons produced in the initial hot deconfined phase by partonic channels is small (of the order of 2%) within our approach [22]. On the other hand, the photons from the hadronic sources show strong elliptic flow (up to 10%), on the level of the v_2 of final hadrons [22]. Accordingly, since the channel decomposition of the direct photons changes, their elliptic flow increases with decreasing centrality and becomes roughly comparable with the v_2 of pions in peripheral collisions. Moreover, the v_2 of the photons increases with decreasing centrality additionally due to the rising of $v_2(b)$ with the impact parameter b, which was observed for all hadrons (except for the most peripheral bin). The increase of the direct photon $v_2(b)$ for the two most central bins has been also indicated in hydrodynamics calculations in Refs. [19,52], although with slightly lower absolute values of v_2. Future measurements of the photon spectra and elliptic flow as a function of the collision centrality will be mandatory for a clarification of the "photon v_2 puzzle" from the experimental side and to estimate the contribution from unconventional sources [20,21,53–56].

Additionally, our calculations have shown that the thermal photon p_T spectra deviate from an exponential distribution at all centralities primarily due to the hadronic bremsstrahlung channels. The effective slopes of these spectra have been extracted in the interval $p_T = 0.4$ to 5 GeV and are constant with centrality within error bars. Due to the nonexponential shape of the photon spectra these effective slopes depend on the fitting interval in p_T; however, they provide effective temperatures significantly above the critical temperature $T_c \approx 160$ MeV for the deconfinement phase transition. Since in PHSD the dominant contributions to the thermal photon yield are related to hadronic bremsstrahlung channels the high slope parameters predominantly reflect the blue-shift of the photon spectra due to the collective flow of hadrons (cf. Ref. [18]). Experimental data at low photon p_T will help in clarifying the physical sources.

Furthermore, since only collisional channels contribute to the production of thermal photons in PHSD, their yield rises faster than the number of participating nucleons $N_{\rm part}$ as expected also from qualitative considerations in Refs. [50,51]. A power-law fit to our results gives approximately a scaling $\sim N_{\rm part}^{\alpha}$ with $\alpha \approx 1.5$, whereas the partonic and hadronic channels separately scale with exponents of $\approx$1.75 and $\approx$1.5, respectively.

We finally point out that respective photon measurements of the ALICE Collaboration at the LHC [57,58] should complete the picture presented in this study. A detailed PHSD analysis of photon production and flow at the LHC collision energies will be reported in the near future.

ACKNOWLEDGMENTS

The authors are grateful for fruitful discussions with B. Bannier, G. David, C. Gale, B. Jacak, L. McLerran, R. Rapp, V. Skokov, A. Toia, V. Toneev, and N. Xu. This work was supported in part by the LOEWE Center HIC for FAIR.

[1] E. V. Shuryak, Sov. Phys. JETP **47**, 212 (1978).
[2] E. V. Shuryak, Phys. Lett. B **78**, 150 (1978); Sov. J. Nucl. Phys. **28**, 408 (1978) [Yad. Fiz. **28**, 796 (1978)].
[3] E. L. Feinberg, Izv. Akad. Nauk Ser. Fiz. **34**, 1987 (1970).
[4] E. L. Feinberg, Nuovo Cim. A **34**, 391 (1976).
[5] J. D. Bjorken and H. Weisberg, Phys. Rev. D **13**, 1405 (1976).
[6] T. Peitzmann and M. H. Thoma, Phys. Rept. **364**, 175 (2002).
[7] P. Aurenche, arXiv:hep-ph/0201011 (2002).
[8] A. Adare *et al.* (PHENIX Collaboration), Phys. Rev. Lett. **109**, 122302 (2012).
[9] A. Adare *et al.* (PHENIX Collaboration), Phys. Rev. C **81**, 034911 (2010).
[10] A. Adare *et al.* (PHENIX Collaboration), Phys. Rev. Lett. **104**, 132301 (2010).
[11] I. Tserruya *et al.* (PHENIX Collaboration), Nucl. Phys. A **904-905**, 225c (2013).
[12] R. Chatterjee *et al.*, Phys. Rev. Lett. **96**, 202302 (2006).
[13] F.-M. Liu, T. Hirano, K. Werner, and Y. Zhu, Nucl. Phys. A **830**, 587C (2009).
[14] M. Dion *et al.*, J. Phys. G **38**, 124138 (2011).
[15] M. Dion *et al.*, Phys. Rev. C **84**, 064901 (2011).
[16] H. van Hees, C. Gale, and R. Rapp, Phys. Rev. C **84**, 054906 (2011).
[17] R. Chatterjee *et al.*, Phys. Rev. C **88**, 034901 (2013).
[18] C. Shen *et al.*, arXiv:1308.2440 (2013).
[19] C. Shen *et al.*, arXiv:1308.2111 (2013).
[20] G. Basar, D. Kharzeev, and V. Skokov, Phys. Rev. Lett. **109**, 202303 (2012).
[21] A. Bzdak and V. Skokov, Phys. Rev. Lett. **110**, 192301 (2013).
[22] O. Linnyk *et al.*, Phys. Rev. C **88**, 034904 (2013).
[23] K. Dusling and I. Zahed, Phys. Rev. C **82**, 054909 (2010).
[24] V. Konchakovski *et al.*, Phys. Rev. C **85**, 044922 (2012).
[25] E. Bratkovskaya *et al.*, Nucl. Phys. A **856**, 162 (2011).
[26] O. Linnyk *et al.*, Phys. Rev. C **84**, 054917 (2011); **85**, 024910 (2012); **87**, 014905 (2013).
[27] V. Konchakovski *et al.*, Phys. Rev. C **85**, 011902 (2012).
[28] W. Cassing and E. L. Bratkovskaya, Nucl. Phys. A **831**, 215 (2009).
[29] E. Bratkovskaya, S. Kiselev, and G. Sharkov, Phys. Rev. C **78**, 034905 (2008).
[30] W. Cassing *et al.*, Phys. Rev. Lett. **110**, 182301 (2013).
[31] S. Turbide, R. Rapp, and C. Gale, Phys. Rev. C **69**, 014903 (2004).
[32] J. I. Kapusta, P. Lichard, and D. Seibert, Phys. Rev. D **44**, 2774 (1991).
[33] C. Gale and J. Kapusta, Phys. Rev. C **35**, 2107 (1987); **38**, 2659 (1988); Nucl. Phys. A **495**, 423c (1989).
[34] O. Linnyk, S. Leupold, and U. Mosel, Phys. Rev. D **71**, 034009 (2005).
[35] O. Linnyk, J. Phys. G **38**, 025105 (2011).
[36] C.-Y. Wong and H. Wang, Phys. Rev. C **58**, 376 (1998).
[37] H. C. Eggers *et al.*, Phys. Rev. D **53**, 4822 (1996).
[38] H. Eggers, C. Gale, R. Tabti, and K. Haglin, arXiv:hep-ph/9604372 (1996).
[39] J. Cleymans, V. Goloviznin, and K. Redlich, Phys. Rev. D **47**, 173 (1993).
[40] SLAC-E-146 Collaboration, P. Anthony *et al.*, Phys. Rev. D **56**, 1373 (1997).
[41] X.-N. Wang, M. Gyulassy, and M. Plumer, Phys. Rev. D **51**, 3436 (1995).
[42] J.-e. Alam *et al.*, Phys. Rev. C **63**, 021901 (2001).
[43] F. D. Steffen and M. H. Thoma, Phys. Lett. B **510**, 98 (2001).
[44] D. K. Srivastava and B. Sinha, Phys. Rev. C **64**, 034902 (2001).
[45] P. Huovinen, P. Ruuskanen, and S. Rasanen, Phys. Lett. B **535**, 109 (2002).
[46] D. G. d'Enterria and D. Peressounko, Eur. Phys. J. C **46**, 451 (2006).
[47] F.-M. Liu *et al.*, Phys. Rev. C **79**, 014905 (2009).
[48] S. Turbide *et al.*, Phys. Rev. C **77**, 024909 (2008).
[49] M. L. Miller, K. Reygers, S. J. Sanders, and P. Steinberg, Ann. Rev. Nucl. Part. Sci. **57**, 205 (2007).
[50] K. Kajantie *et al.*, Phys. Rev. D **34**, 2746 (1986).
[51] D. K. Srivastava and K. Geiger, Nucl. Phys. A **661**, 592 (1999).
[52] A. Chaudhuri, arXiv:1305.6121 (2013).
[53] V. Goloviznin, A. Snigirev, and G. Zinovjev, JETP Lett. **98**, 61 (2013).
[54] Y. Yin, arXiv:1312.4434 (2013).
[55] B. Müller, S.-Y. Wu, and D.-L. Yang, arXiv:1308.6568 (2013).
[56] V. Skokov, J. Phys. Conf. Ser. **432**, 012021 (2013).
[57] M. Wilde (ALICE Collaboration), Nucl. Phys. A **904-905**, 573c (2013).
[58] D. Lohner (ALICE Collaboration), J. Phys. Conf. Ser. **446**, 012028 (2013).